$SrFeO_{3-\delta}$ Assisting with Pd Nanoparticles on the Performance of Alcohols Catalytic Oxidation

Yavari, Zahra; Noroozifar, Meissam*+; Mirghoreishi Roodbaneh, Mahsa; Ajorlou, Bahram

Department of Chemistry, University of Sistan and Baluchestan, P.O. Box 98135-674 Zahedan, I.R. IRAN

ABSTRACT: *Current catalysts for the alcohol oxidation in fuel cells (typically noble metals-based) are susceptible to poisoning with intermediates like CO. Hence we decided to find superseded catalysts for methanol oxidation based on incorporation of mixed oxides. In this research, a nano-size perovskite $SrFeO_{3-\delta}$ ($SrFeO_{3-\delta}$NPs) was synthesized by a rapid co-precipitation method assisted with ultrasonic and characterized by XRD, FT-IR, SEM and EDX techniques. A modified glassy carbon electrode with Pd nanoparticles (PdNPs) and $SrFeO_{3-\delta}$NPs dispersed into the appropriate amount of chitosan (CH) polymer as a multifunctional catalyst was prepared and its catalytic activity toward alcohols (C_1 - C_3) oxidation was investigated. Based on the electrochemical studies, the PdNPs-$SrFeO_{3-\delta}$NPs-CH nanocomposite showed considerable activity for alcohols (C_1 - C_3) oxidation in comparison to PdNPs-CH and $SrFeO_{3-\delta}$NPs-CH. A direct methanol fuel cell was designed, assembled and tested with suggested PdNPs-$SrFeO_{3-\delta}$NPs-CH nanocomposite under several different conditions. The effect of experimental parameters (temperature; methanol concentration; flow rate) as well as NaOH concentration) on the electrical performances of the fuel cell were studied and optimized.*

KEYWORDS: *Perovskite; Palladium; Alcohol oxidation; Fuel cell; Nanocatalyst*.

INTRODUCTION

Today, the use of Direct Alcohol Fuel Cells (DAFCs) is increased as a supplementary power source for various applications [1]. Among diverse compounds; alcohols (C_1-C_3) are examined as fuel for these fuel cells [2-4]. However, the aspect of the methanol toxicity is important but it is applied as a primary fuel for DAFC because of its low cost and simple storage. While ethanol has a higher cost, it is also considered an attractive choice fuel for the reason that it has low toxicity and can be produced from a wide-ranging variety of biomass products [5]. The DAFCs as low-temperature fuel cells use platinum or it's alloys as electrode materials. Palladium has a similar lattice constant and valence shell electronic configuration to platinum [6]. In view of both aspects of price and performance, palladium can be a suitable material for low-temperature fuel cells. It is the most frequently employed catalyst material for anode reactions in direct alcohol fuel cell [7, 8] but their performance is limited by basic problems, including kinetics restraints and poisoning [9]. It is necessary to consider novel catalyst materials providing good electrical conductivity, catalysis along with reducing the poison substitute for noble metal.

***** *To whom correspondence should be addressed.*
+ E-mail: mnoroozifar@chem.usb.ac.ir
1021-9986/2017/5/21-37 17/$/6.70

In most cases, the necessities of support materials for their applications to the supports for noble metal-based catalyst are a high surface area for well-dispersion of nanocatalysts, low electrical resistance to make easy electron transport during the electrochemical reactions, an appropriate porous structure for upper limit contact with fuel or oxidant and powerful interaction between the catalyst and the support [10]. Particularly, oxide supports are used in heterogeneous catalysis extensively and have higher stability inherently than carbon in oxidizing environments. Perovskite (ABO_3) is a versatile catalyst which has been used in different fields such as exhaust abatement and CO, methane, and methanol oxidation. It can be attributed to its thermal stability, unique crystalline structure and ion mobility [11]. *Varma et al.* [12] found that the performance of Sr-based perovskites in DMFCs is comparable with Pt-Ru catalysts. They also indicated that the catalytic activity of Pt will be enhanced in presence of $SrRuO_3$. In another study, the perovskite / platinum catalysts ($SrRuO_3$-Pt and $LaRuO_3$-Pt) which contain much less Pt than those for standard ones, have been suggested as low-cost and multifunctional catalysts [13]. Natural polymers such as chitosan (CH) permit uniform distribution of catalyst particles, which forms the major criteria of catalytic reactions. They can be employed as host matrixes to integrate noble metal nanocatalysts for their possible applications in the oxidation of molecules such as hydrogen and alcohol (C_1 - C_3) [8]. Polymers such as chitosan and nafion are well-situated supports for dispersing catalytic materials at the molecular level [14].

In this paper, in order to provide more effective reaction sites for the catalysis; $SrFeO_{3-\delta}$ perovskite catalysts were synthesized as nano-meter particles ($SrFeO_{3-\delta}$NPs). The activity of palladium nanoparticles (PdNPs) in the presence of $SrFeO_{3-\delta}$NPs for alcohols (C_1 – C_3) oxidation was evaluated by the electrochemical techniques. Multifunctional nanocatalysts, PdNPs, $SrFeO_{3-\delta}$NPs and PdNPs-$SrFeO_{3-\delta}$NPs dispersed in chitosan (CH) were successfully prepared and their catalytic activity toward alcohols (C_1 – C_3) oxidation was compared with each other. The effect of experimental factors on the anodic current density and the potential of alcohols (C_1 – C_3) oxidation were studied. Finally, the function of the PdNPs-$SrFeO_{3-\delta}$NPs-CH nanocomposite was investigated in the stack and assembled direct methanol fuel cell as anodic catalysts. The fuel cell polarization curves were plotted for the mentioned single cell.

EXPERIMENTAL SECTION

Materials

Strontium chloride ($SrCl_2.6H_2O$), ferric chloride ($FeCl_3.6H_2O$), palladium chloride ($PdCl_2$), sodium borohydride ($NaBH_4$), sulfuric acid (H_2SO_4), oleic acid ($C_{18}H_{34}O_2$) and sodium hydroxide (NaOH) were obtained from Merck. 1% acetic acid solution was prepared with water. A natural polymer, Chitosan, ([2-amino-2-deoxy-(1-4)-β-D-glucopyranose]), contains medium molecular weight (~ 400,000 Da) was obtained from Fluka. All reagents were used without additional purification. The Carbon Cloth - Diffusion Layer (CC-DL) and Nafion membrane were purchased from Asian Hydrogen New Science Company; manufacturing & development Isfahan Science and Technology Town, Isfahan, Iran. All solutions were prepared by doubly distilled water.

Instrumentation

The catalytic activity of introduced nanocomposites was studied using the electrochemical techniques in a conventional cell with three-electrode at room temperature. The working electrode substrate was a GC electrode with 0.03 cm^2 surface area. A platinum electrode as the counter electrode and also a Hg/HgO electrode as the reference electrode were used. The electrolyte was a mixture of potassium hydroxide (KOH) and the corresponding methanol with a known concentration. All experiments were performed at room temperature. A sonicator Euronda-Eurosonic (4D Model) was employed for ultrasound-assisted co-precipitation. The analysis of X-ray diffraction was conducted on a Philips analytical PC-APD X-ray diffractometer accompanied graphite monochromatic CuK_α radiation (λ = 1.54 Å) to verify the formation of products. The spectra of Fourier transform infrared of the materials were taken using a JASCO-460 FT-IR spectrometer. As well as, the surface morphology and the status of the nanoparticles were characterized by scanning electron microscopy and energy dispersive X-ray analysis, which was equipped with an SEM instrument (SEM-Philips XL30). TEM image was taken using a Philips CM120 transmission electron microscopy with 2.50 Å resolution. An air brush kit model MBD-116C was employed for spray nanocatalyst ink on CC-DL.

Preparation of $SrFeO_{3-\delta}$ nanocrystalline

$SrFeO_{3-\delta}$ nanoparticles were synthesized by our reported [15] but here oleic acid was used instead of octanoic acid as surfactant and also, ultrasonic assisted co-precipitation method was employed in place of the microwave. Aqueous solutions of 0.1 M ferric chloride ($FeCl_3.6H_2O$) and 0.1 M strontium chloride ($SrCl_2.6H_2O$) were prepared and mixed together in 1:1 molar ratio. Deionized distilled water was employed as the solvent in order to avoid the production of impurities in the resulted product. 2 mL oleic acid was added to the mixture as a surfactant. The solution was stirred followed along with adding NaOH solution (1.5 M) drop by drop to keep the p*H* at 7 - 8. After complete precipitation, the liquid precipitate was irradiated with ultrasonic waves. The sonication time was found effective in the formation of the crystalline phase of perovskite nanoparticles. In this experimental conditions were 15 min / 60 ˚C (250 W and 40 kHz). After cooling at room temperature, the products were centrifuged for 15 min at 403 RCF and washed with distilled water and ethanol numerous times to remove the excess surfactant from the solution. The product was calcinated at 800 ˚C for 6 h to let the product self-ignite and also burn off the organic compound in the material. The product was cooled to room temperature and the $SrFeO_{3-\delta}$NPs were obtained.

Preparation of nanocomposites

A chitosan solution (2 mg/mL) in 1% acetic acid solution was prepared, due to the poor solubility of the polymer, the mixture was stirred to dissolve entirely and kept for 24 h, and the solution was filtrated to remove any impurity before use. 25 µL 37% HCl solution was added to 5 mg of $PdCl_2$ salt. During this mixture, Pd^{+2} ions were transformed to $PdCl_4^{-2}$ which has better solubility. The result was mixed with a known amount of CH solution with a rotary aperture (200 rpm) for 50 min. Then, 50 µL of a freshly prepared aqueous solution of 2.5 M $NaBH_4$ was added to the blend. It was kept stirring for 60 min to achieve complete reduction of Pd nanoparticles (Eq. (1)).

$$4NaBH_4 + H_2PdCl_4 \rightarrow Pd + 4NaCl + 2B_2H_6 + 3H_2 \quad (1)$$

The resulting suspension (PdNPs-CH) was kept at room conditions for consecutive studies. 2 mg $SrFeO_{3-\delta}$NPs was added to 0.5 mL CH solution and mixed with using an ultrasonic bath for 15 min ($SrFeO_{3-\delta}$NPs-CH).

Electrode preparation

The GC electrode with 0.03 cm^2 surface area was polished with 0.05 µm alumina slurry to a mirror finish surface and was then rinsed with distilled water. The GC electrode was cleaned and activated in an electrochemical cell containing 1 M H_2SO_4 solution by using cyclic voltammetry (CV) technique between −1.5 and +1.5 V at a scan rate of 100 mV/s until a stable voltammogram profile (~ 15 times) was obtained. The clean electrode was modified with 'layer by layer' method. For electrode modification, 10 µL PdNPs-CH was spread by a pipette onto the prepared GC electrode and the electrode was put under infrared radiation for 10 min. Then, 10 µL $SrFeO_{3-\delta}$NPs-CH was spread onto the prepared electrode. The prepared electrode was kept under infrared radiation for 10 min. During this period, the solvent evaporation led to the formation of a deposited catalyst layer on the GC electrode surface. This modified GC electrode has been denoted as GC/PdNPs-$SrFeO_{3-\delta}$NPs-CH. The GC/PdNPs-CH and GC/$SrFeO_{3-\delta}$NPs-CH were also prepared with the same process.

CO stripping

The reaction of CO oxidation on the modified electrodes was evaluated with using the CO stripping technique. CO is adsorbed at a constant potential (~ 50 mV) during 15 min. In the following, N_2 gas is purged to remove dissolved CO during 30 min. The potentials scan at 50 mV/s between -0.6 and 0.4 V vs. Hg/HgO was recorded for each of the electrodes.

Single cell test

Initially, the prepared suspension nanocatalysts were sprayed uniformly onto CC-DL by using the airbrush kit. The anode catalyst loading was (2 mg/cm^2) PdNPs - (1 mg/cm^{-2}) $SrFeO_{3-\delta}$NPs onto the CC-DL (PdNPs-$SrFeO_{3-\delta}$NPs-CH/CC-DL); whereas the active surface area of the single cell was about 5 cm^2. The PtNPs-CH was first prepared as indicated in "Preparation of Nanoparticles" section from the chloride precursor (Eq. (2)) then sprayed onto CC-DL.

$$6NaBH_4 + H_2PtCl_6 \rightarrow Pt + 6NaCl + 3B_2H_6 + 4H_2 \quad (2)$$

The CC-DL with prepared PtNPs-CH with 4 mg/cm^2 Pt-loading was used as cathode. A Nafion117 membrane was pretreated by successive dipping in 5% wt H_2O_2

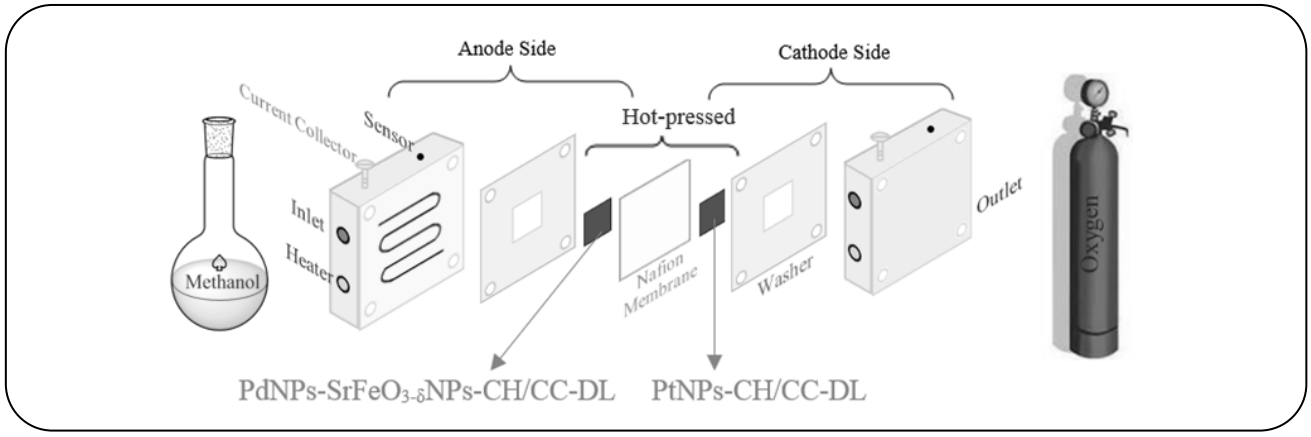

Scheme 1: The single cell assembling of direct methanol fuel cell.

solution, doubly distilled water, 8% wt H_2SO_4 solution and finally in the doubly distilled water again, at 80 °C, 30 min each step. The diffusion layers based on carbon cloths with prepared catalyst layers on the anode and the cathode sides and membrane in the middle were formed the single cell. Hot-pressing is known as an essential step for the preparation of the Membrane Electrode Assembly (MEA) fabricated in this method. Higher catalyst utilization, suitable contact between the membrane and the catalyst layer, which can effectively reduce the catalyst loading without sacrificing the MEA performance, all play an effective role. In a MEA, the Gas Diffusion Layers (GDLs) with catalyst layers are directly applied to both sides of the pre-treated Nafion membrane with hot-pressed. The anode and cathode layers were hot-pressed onto both sides of the Nafion 117 membrane between two ceramic papers at 120 ˚C and 200 psi for 4 min. The MEA was assembled in the single cell for performance evaluation (Scheme 1). The flow rate of methanol as fuel was controlled using a peristaltic pump. *I–V* curves were obtained with an electronic load, EL200P, Daegil, galvanostatically and controlled via a personal computer.

RESULT AND DISCUSSION

Characterization of $SrFeO_{3-\delta}$NPs

Fig. 1A shows the FT-IR spectra of oleic acid (up), the product before calcination (medial), and $SrFeO_{3-\delta}$NPs perovskite after calcination (bottom), in the frequency range from 4000 to 400 cm^{-1}. In Fig. 1A (up spectrum), the 2500-3400 cm^{-1} broad band can be attributed to the stretching vibration of oleic acid O-H bond. The absorptive peak at 3006 cm^{-1} is characteristic bands of the =C-H group. While the peak at 1710 cm^{-1} is the typical band of the carbonyl group. The bands at 1465 and 1378 cm^{-1} can be related to the bending of CH_2 and CH_3 bonds, respectively. The absorption peak detected at 1285 and 938 cm^{-1} are attributed to the stretching of C-O and out of plane bending of the O-H group, respectively. The peaks at 700-800 cm^{-1} arose from out of plane bending of the =C-H group. For a precursor, all infrared bands of oleic acid are observed but shifted to a lower wave number as seen in Fig. 1A (middle spectrum). In the FT-IR spectrum of the final product (bottom spectrum), two strong absorptive bands at nearby 555 and 439 $cm^{-1}$are correspond to M–O stretching vibration and O–M–O bending vibration of $SrFeO_{3-\delta}$NPs, respectively (M: Metal).

Fig. 1B shows the XRD pattern of $SrFeO_{3-\delta}$ perovskite. The analysis of XRD pattern was matched to perovskite-type $SrFeO_{3-\delta}$ (JCPDS File no. 40-0905), which crystallizes in the orthorhombic system with main diffraction peak at d = 2.71 Å ((0 1 1) plane). The sharpening of the peaks is due to the high crystallinity of the $SrFeO_{3-\delta}$NPs. The peak broadening confirmations in XRD patterns show that the $SrFeO_{3-\delta}$ particles are nano-sized. The mean size of the $SrFeO_{3-\delta}$NPs (D) was estimated by XRD line broadening [16]:

$$D = \frac{0.89 \times \lambda}{\beta \times \cos\theta} \quad (3)$$

where D is the average grain size, λ = 1.54 Å and β is the width of the peak of the diffraction at half maximum for the diffraction angle 2θ. Based on the line width for the diffraction peaks positioned at 2θ = 32.74˚, we estimate the average crystallite size to be ~37 nm.

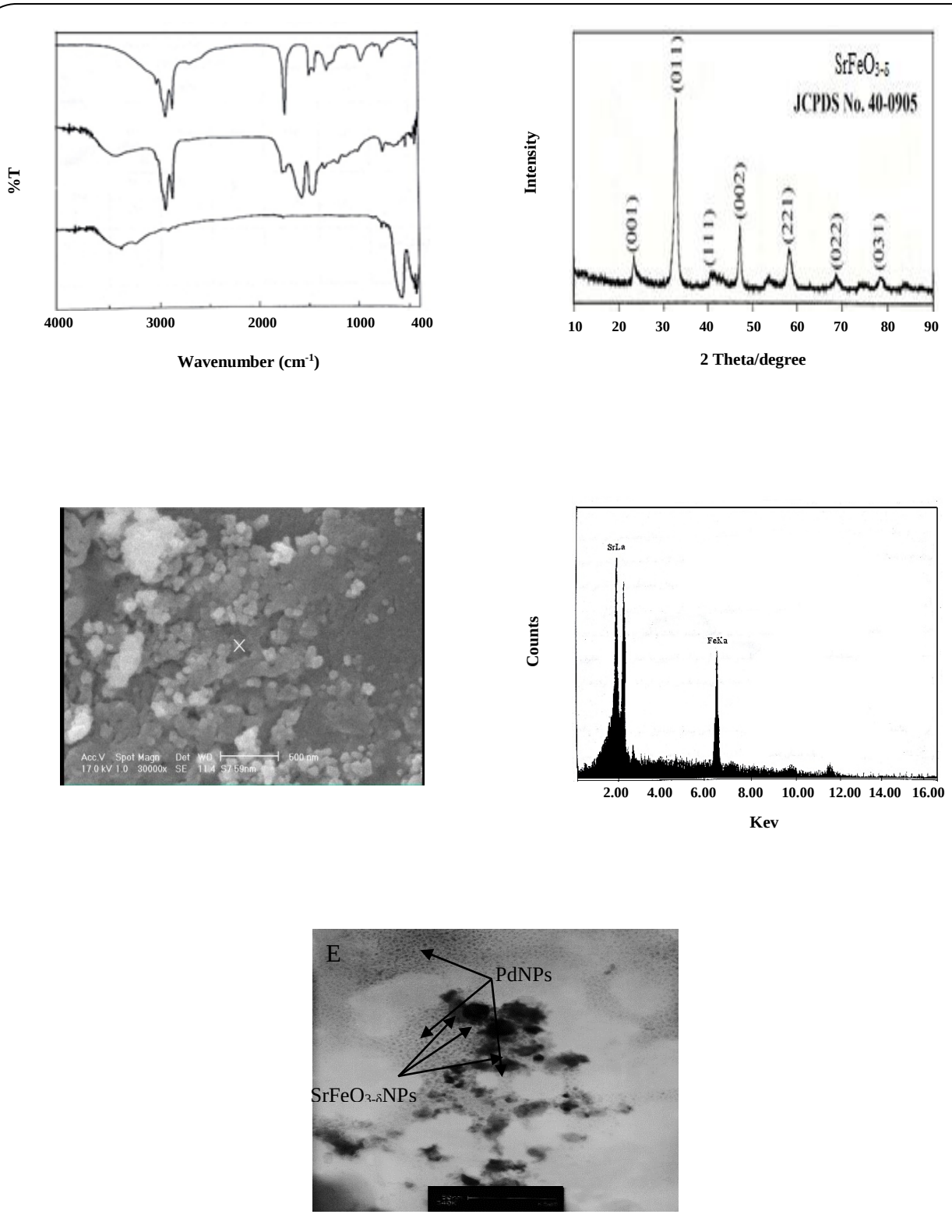

Fig. 1. (A) FT-IR spectra of oleic acid (up), product before (middle) and after (bottom) calcination, (B) XRD, (C) SEM, (D) EDX pattern of $SrFeO_{3-\delta}$NPs and (E) TEM image of PdNPs-$SrFeO_{3-\delta}$NPs-CH.

To investigate the size and morphology of the perovskite nanoparticles, scanning electron microscopy (SEM) was also used. The SEM image of the particles is shown in Fig. 1C. The mean sphere-like particle size is approximately 59 nm. The SEM image shows that there are several holes in the nanoparticles, which indicate that it can be used in catalysis. In the SEM image, the presence of holes showed perovskite as a porous material. The perovskite has a large fraction of metal atoms at surface available for dispersion of PdNPs due to its high surface-to-volume ratio. It is clear that the surface area is an important parameter in heterogeneous catalysis. The holes in perovskite develop fuel storage for consumption on the catalyst surface. EDX was performed on $SrFeO_{3-\delta}$NPs for more demonstrations. The EDX spectrum given in Fig. 1D shows the presence of strontium and ferric as the component elements.

Characterization of PdNPs-SrFeO$_{3-\delta}$NPs-CH catalyst

Fig. 1E displays the TEM micrograph of the PdNPs-$SrFeO_{3-\delta}$NPs-CH composite. It was realized from Fig. 1E that PdNPs with sizes of 2 – 4 nm and $SrFeO_{3-\delta}$NPs were uniformly distributed.

One of the important parameters for the determination of catalytic activity of nanocomposites is the Electrochemical Active Surface (EAS) area of PdNPs, especially for surface reactions like the oxidation of heterogenic catalysis. The EAS is calculated from H_2 adsorption/desorption on PdNPs in different catalyst PdNPs-CH and PdNPs-$SrFeO_{3-\delta}$NPs-CH using cyclic voltammetry technique. Fig. 2A displays the cyclic voltammograms of the GC/PdNPs-CH (curve a) and GC/PdNPs-$SrFeO_{3-\delta}$NPs-CH (curve b) electrodes in 1 M KOH solution at the potential range of -1 to 0.6 V (vs. Hg/HgO) with palladium loading of 0.31 mg/cm^2. In actuality, the CV curve in the absence of alcohol was attributed to the double layer region of the modified electrodes. The characters of the cyclic voltammograms were in excellent accordance with those reported for noble metal-based catalysts [17, 18]. When the electrode potential is ramped to a more positive potential (with respect to Hg/HgO) linearly, protons and electrons are produced from the oxidation of the adsorbed hydrogen on PdNPs surface;

$$Pd-H_{abs/ads}+OH^- \rightarrow Pd+H_2O+e^- \quad (4)$$

Based on the literature, the first anodic peak and the last cathodic peak in Fig. 2A correspond to desorption of adsorbed hydrogen, respectively [19]. Also, the PdNPs oxide such as PdO, PdOH, $Pd(OH)_2$ and PdO_2 was formed in the positive potential region [20]. The peak centering at -0.4V vs. Hg/HgO in the cathodic sweep was corresponded to the reduction of the palladium oxide.

$$Pd-O+H_2O+2e^- \rightarrow Pd+2OH^- \quad (5)$$

The columbic charge (Q_H) of the hydrogen desorption is employed for calculation of palladium Electrochemically Active Surface (EAS) area of the electrodes. Q_H is the mean value between the amounts of charge exchanged during the electrochemical adsorption of hydrogen molecules (Q'_H) and their desorption (Q''_H) of on the Pd sites [21].

$$Q_H=\frac{Q'_H+Q''_H}{2} \quad (6)$$

It was calculated by determining the area under the peak at the potential range of hydrogen adsorption/desorption on the prepared electrodes. The EAS is calculated by Equation (7):

$$EAS=\frac{Q_H}{k\times l} \quad (7)$$

where Q_H is the columbic charge during the electrochemical adsorption and desorption of hydrogen on Pd sites, l is the palladium loading (mg/cm^2) on the electrode and k is a parameter relating the charge to the area; A charge value 4.2 C/m^2 is assumed for oxidation of a monolayer of H_2 on PdNPs. The Q_H is 108.99 and 155.73 mC/cm^2 for GC/PdNPs-CH and GC/PdNPs-$SrFeO_{3-\delta}$NPs-CH electrodes, respectively. The Q_H for GC/PdNPs-CH and GC/PdNPs-$SrFeO_{3-\delta}$NPs-CH are more than that of Pd nano wire array with 10.6 mC/cm^2 and Pd film with 3.4 mC/cm^2 columbic charge for 0.24 and 1.10 mg/cm^2 palladium loading [22]. The EAS was calculated 83.17 and 118.84 m^2/g for GC/PdNPs-CH and GC/PdNPs-$SrFeO_{3-\delta}$NPs-CH electrodes, respectively. It is shown that the addition of $SrFeO_{3-\delta}$NPs to PdNPs-CH nanocomposite increased the EAS amount. As a result of the great EAS, the GC/PdNPs-$SrFeO_{3-\delta}$NPs-CH electrode has an improved dispersion and less size of PdNPs. The same result was reported for hydrogen adsorption on oxides with more oxidized metal centers (e.g. Fe ions) by *Tejuca* [23].

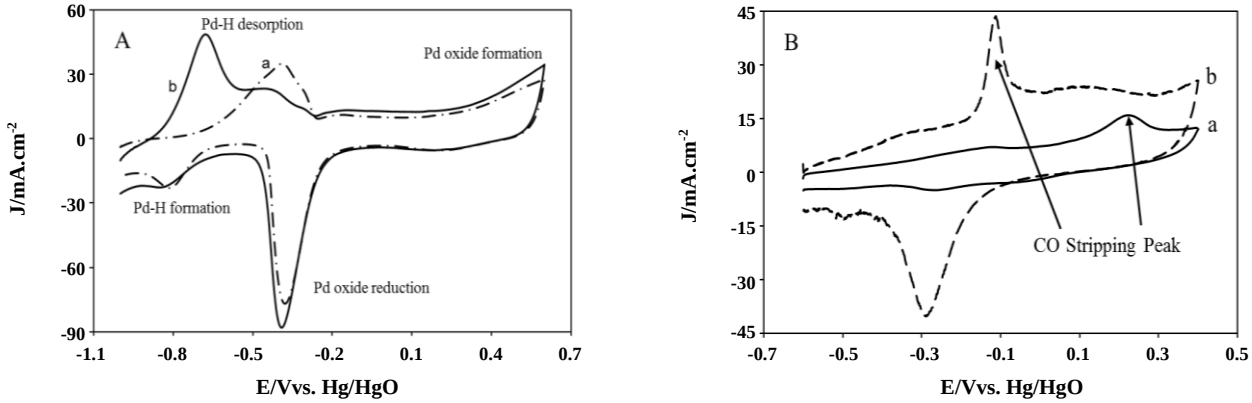

Fig. 2: (A) The cyclic voltammograms and (B) CO stripping curves of (a) GC/PdNPs-CH and (b) GC/PdNPs-$SrFeO_{3-\delta}$NPs-CH electrodes with the palladium loading of 0.31 mg/cm^2 in 1 M KOH solution.

During the forward scans on catalysts containing perovskite, the current density was raised along the entire investigated potential range. The dispersion of PdNPs was defined as a fraction of surface-active Pd atoms in all of the Pd atoms which can be achieved [24]:

$$D_{Pd} = \frac{EAS}{\frac{1}{M_{PD}} \times \left(N_A \times 4\pi \times r_{Pd}^2 \right)} \quad (8)$$

where M_{Pd} is the relative molecular weight of Pd (106.42 g/mol), N_A is Avogadro number (6.02×10^{23}) and r_{Pd} is Pd atomic radius (0.14 nm). D_{Pd} was estimated more 1.43 times with the $SrFeO_{3-\delta}$NPs adding, approximately. It is clear that both the synergistic effect of PdNPs and structure effects of the $SrFeO_{3-\delta}$NPs enhanced the catalytic activity of the PdNPs-$SrFeO_{3-\delta}$NPs-CH nanocomposite for alcohol oxidation.

Furthermore, accelerated durability test (ADT) of the nanocatalysts was carried out by continuously applying potentials between -1 to 0.6 V vs. Hg/HgO with a scan rate 50 mV/s in 1 M KOH after 100 potential cycles. In general, the durability of the modified electrode was tested by performing the potential cycling as ADT in alkaline solution. The voltammogram of H_2 adsorption/desorption was used to determine the change of the PdNPs electrochemical surface area for modified electrodes by comparing H_2 desorption regions before and after 100 potential cycles. The EAS value for both electrodes was decreased (from 83.17 to 59.88 m^2/g for GC/PdNPs-CH and from 118.84 to 91.51 m^2/g for GC/PdNPs-$SrFeO_{3-\delta}$-CH electrode) after the ADT. The obtained %ADT parameter is calculated from Eq. (9):

$$\%ADT = \frac{\left(EAS_{run1} - EAS_{run100} \right)}{EAS_{run1}} \times 100 \quad (9)$$

It was calculated 28.02 and 22.98 % for GC/PdNPs-CH and GC/PdNPs-$SrFeO_{3-\delta}$-CH electrodes after 100 potential cycle, respectively. Consequently, the D_{Pd} value for the mentioned electrode decreases after ADT, indicating a notable decrease of the PdNPs active surface area due to Pd sintering and the dissolution of Pd metal.

The recorded cyclic voltammograms of both modified electrodes during the reaction of CO oxidation are represented in Fig. 2B. Three considerable differences between voltammograms of the modified electrode are detected:

1) The onset potential of the CO stripping peak for GC/PdNPs-$SrFeO_{3-\delta}$NPs-CH (= -0.60 V vs. Hg/HgO) is shifted by about 0.02 V positive versus that at a GC/PdNPs-CH (= -0.57 V vs. Hg/HgO) electrode.

2) The current density of the CO stripping peak for GC/PdNPs-$SrFeO_{3-\delta}$NPs-CH (= 42.87 mA/cm^2) is more than other electrode (=15.99 mA/cm^2) electrode.

3) The potential peak of the CO stripping reaction for GC/PdNPs-$SrFeO_{3-\delta}$NPs-CH (= -0.11 V vs. Hg/HgO) is shifted by about 0.34 V positive versus GC/PdNPs-CH (= +0.23 V vs. Hg/HgO) electrode.

The $Q_{CO,ads}$ was 12.08 and 32.57 mC/cm^2 for GC/PdNPs-CH and GC/PdNPs-$SrFeO_{3-\delta}$NPs-CH electrodes, respectively. This difference is attributed to the removal of CO poisoning on the PdNPs surface by the surface oxygen of the $SrFeO_{3-\delta}$NPs perovskite that was in adjacency of metal particles.

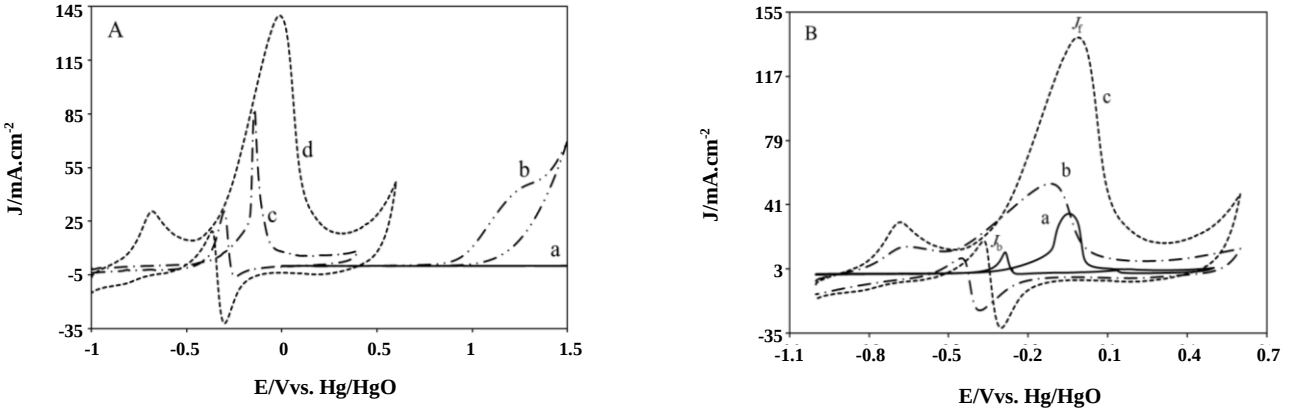

Fig. 3: (A) Cyclic voltammograms on (a) GC and GC/CH (b) GC/SrFeO$_{3-\delta}$NPs-CH, (c) GC/PdNPs-CH and (d) GC/PdNPs-SrFeO$_{3-\delta}$NPs-CH electrodes in 0.64 M methanol, (B) Cyclic voltammograms of (a) 0.42 M isopropanol, (b) 0.55 M ethanol and (c) 0.64 M methanol at GC/PdNPs-SrFeO$_{3-\delta}$NPs-CH electrode in 1 M KOH.

Also, the Electrochemical Active Surface Area (ECSA) of the catalysts can be determined by using estimating the area under the curve of palladium oxide reduction (Q_p) using the following equation [25]:

$$\mathrm{ECSA} = \frac{Q_p}{k \times l} \quad (10)$$

where Q_p is the columbic charge in mC and determined by calculating the area under the curve of the palladium oxide reduction. A proportionality constant, k = 0.405 mC cm^{-2} is considered for the charge required for reduction of palladium oxide monolayer and l is the loading of Pd on the surface of the electrode in mg/cm^2. ECSA values were found to be 160.30 and 183.84 m^2/g for GC/PdNPs-CH and GC/PdNPs-SrFeO$_{3-\delta}$NPs-CH electrodes, respectively. The results show that the ECSA of PdNPs-SrFeO$_{3-\delta}$NPs-CH is higher than PdNPs-CH, indicating developed catalytic activities and also more effective utilization of Pd nanoparticles over the surface.

Alcohols (C$_1$-C$_3$) oxidation on GC/PdNPs-SrFeO$_{3-\delta}$NPs-CH electrode

The catalytic activity of modified electrodes for methanol oxidation have been investigated by cyclic voltammetry, Controlled potential coulometry (amperometric curve) and Anodic Tafel polarization techniques in a known alcohol and 1 M NaOH aqueous solution.

Cyclic voltammetry

Fig. 3A represents the cyclic voltammograms for different electrodes such as the GC, GC/CH, GC/PdNPs-CH, GC/SrFeO$_{3-\delta}$NPs-CH and GC/PdNPs-SrFeO$_{3-\delta}$NPs-CH in 1 M KOH and 0.64 M methanol solution at a scan rate of 50 mV/s. Based on Fig. 3A, GC, and GC/CH electrodes (Fig. 3A, curve a) do not show any peaks for the oxidation of methanol. It has been known that GC and GC/CH electrodes cannot have any catalytic activity for methanol oxidation. The appearance of the methanol oxidation peak at 1.26 V vs. Hg/HgO for GC/SrFeO$_{3-\delta}$NPs-CH confirmed the catalytic activity of the perovskite nanoparticles but this positive potential peak is not suitable for quick start-up of the fuel cell. The cyclic voltammogram at the GC/PdNPs-SrFeO$_{3-\delta}$NPs-CH electrode (Fig. 3A curve d) for methanol oxidation indicates that there is a great enhancement in current density during the forward scan in comparison to GC/PdNPs-CH (Fig. 3A curve c). This result shows that the GC/PdNPs-SrFeO$_{3-\delta}$NPs-CH electrode has a suitable catalytic activity for methanol oxidation reaction in DMFC.As seen from Fig. 3A (curves c and d), two oxidation peaks, which are associated with the oxidation of methanol (J_f) and the corresponding intermediates (J_b) were produced during the oxidation of methanol (J_f / J_b = 7.33 and 2.88), which can be observed at 0.00 and -0.15 V (E_f) and -0.37 and -0.30 V (E_b) vs. Hg/HgO for GC/PdNPs-SrFeO$_{3-\delta}$NPs-CH and GC/PdNPs-CH, respectively. Fig. 3B represents cyclic voltammograms for the oxidation of 0.64 M methanol, 0.55 M ethanol and 0.42 M isopropanol on the GC/PdNPs-SrFeO$_{3-\delta}$NPs-CH electrode in 1 M KOH solution at scan rate of 50 mV/s and the potential range of -1 to 0.6 V vs. Hg/HgO.

Table 1: Electrochemical data for alcohols (C_1–C_3) oxidation on GC/PdNPs-$SrFeO_{3-\delta}$NPs-CH electrode.

Alcohol	Concentration (M)	Onset potential (V vs. Hg/HgO)	E_f (V vs. Hg/HgO)	J_f (mA/cm^2)	E_b (V vs. Hg/HgO)	J_b (mA/cm^2)	J_f / J_b
Methanol	0.64	-0.91	+0.00	138.88	-0.37	18.95	7.33
Ethanol	0.55	-0.91	-0.12	53.33	-0.45	9.18	5.81
Isopropanol	0.42	-0.53	-0.05	35.75	-0.29	12.64	2.83

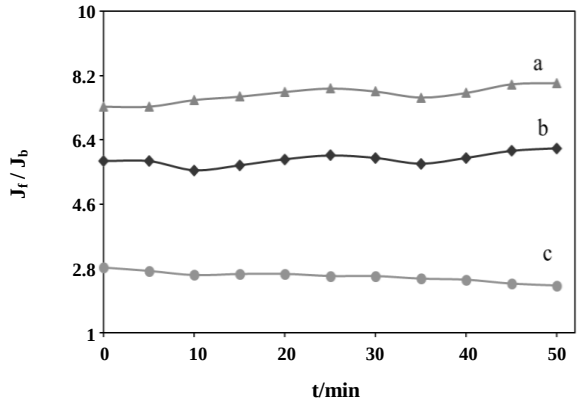

Fig. 4: The plot of J_f / J_b ratio as a function of time for the oxidation of (a) 0.64 M methanol, (b) 0.55 M ethanol and (c) 0.42 M isopropanol on GC/PdNPs-$SrFeO_{3-\delta}$NPs-CH electrode in 1 M KOH.

Table 1 directs the quantitative analyses on CV curves for alcohol (C_1-C_3) oxidation on GC/PdNPs-$SrFeO_{3-\delta}$NPs-CH electrode. The amount of the onset potential for methanol oxidation as the anodic reaction is important for DMFC. The variation in the onset potential relates to an improvement in the kinetics of methanol oxidation [26]. The GC/PdNPs-$SrFeO_{3-\delta}$NPs-CH electrode had the less value of onset potential than the Pt/RuO_2 [27] and Pt/WO_3 [28] for methanol oxidation.

This point shows that the $SrFeO_{3-\delta}$NPs incorporation improves the kinetics of alcohol oxidation reaction and effects on fuel cell start-up. The current density on GC/PdNPs-$SrFeO_{3-\delta}$NPs-CH electrode is comparable with others containing noble metals or perovskite electrodes [29, 30]. These results explain that PdNPs-$SrFeO_{3-\delta}$NPs-CH nanocomposite has a suitable activity for alcohol (C_1-C_3) oxidation in alkaline media. The ratio of forward and reverse peak current densities is used to compare the activity of synthetic catalysts for alcohol oxidation which is determined as J_f / J_b in Table 1. This has been used to determine the tolerance of such catalysts to CO, an intermediate of methanol oxidation; with larger values regarded as a positive sign that the nanocomposite is an excellent CO resistant catalyst [31].The high J_f / J_b ratio could be attributed to the removal of CO poisoning on the Pd surface by the surface oxygen of $SrFeO_{3-\delta}$ perovskite nanoparticles that is in adjacent to metal particles [32].

In order to examine the poisoning effect of as-prepared electrodes during alcohol oxidation reaction, the catalytic activity of GC/PdNPs-$SrFeO_{3-\delta}$NPs-CH electrode is investigated through cyclic voltammetry repeatedly. Fig. 4 showed the J_f / J_b ratios as a function of time. As observed for GC/PdNPs-$SrFeO_{3-\delta}$NPs-CH electrode, J_f / J_b is approximately stabled during 50 min, indicating the suitable anti-poisoning performance of this catalyst for the oxidation of three alcohols. There was a gradual drop of J_f / J_b ratio within the first 10 min, whereas the J_f / J_b ratios of methanol and ethanol oxidation, exhibited an increasing trend after 35 min. PdNPs-$SrFeO_{3-\delta}$NPs-CH catalyst had the highest J_f / J_b ratio after 50 min for methanol oxidation, indicating that this catalyst is capable of offering excellent anti-poisoning effect toward oxidation of simpler alcohols without C-C bond.

Anodic Tafel polarization

The intrinsic activity of PdNPs-$SrFeO_{3-\delta}$NPs-CH nanocomposite was measured towards the alcohol (C_1-C_3) oxidation at 50 mV/s in room temperature and alkaline media. The values of the exchange current density (J_0) and polarization resistance (R_p) at Table 2 were obtained by extrapolating the Tafel line to the equilibrium potential (E_{eq}) for the alcohol oxidation reaction in 1 M KOH solution. The amount of the Tafel slope was calculated from the linear portions of a log current density vs. potential plot ($b \approx 100$ mV/dec). It was dependent on the coverage of pre-adsorbed CO on the alcohol oxidation as an anodic reaction. The value of the Tafel slope demonstrates the adsorption of alcohol on the rare earth-including catalyst was more difficult compared to that on the noble metals [30].

Table 2: The results of polarization curve for the alcohols ($C_1 - C_3$) oxidation on GC/ PdNPs-$SrFeO_{3-\delta}$NPs-CH electrode.

Alcohol	C (M)	E_{eq} (V vs. Hg/HgO)	J_0 (mA/cm^2)	R_p (ohm)
Methanol	1.68	-1.08	1.25	551.50
Ethanol	0.23	-1.01	0.48	1443.00
Isopropanol	0.17	-0.96	0.40	1728.00

Also, *Tripković et al.* [33] explained that several factors such as electrode surface structure, surface absorbents, p*H* values and their interactions are of great importance for the Tafel slope determination. The J_0 value is correlated to the real electrochemical surface area of the modified electrode. Also, polarization resistance (R_p) could be a criterion for charge exchange on the surface anodic catalyst. The J_0 value of GC/PdNPs-$SrFeO_{3-\delta}$NPs-CH electrode was higher than the reported values in the literature for methanol oxidation [34]; which shows that larger exchange current density leads to the faster reaction by the mentioned catalysis.

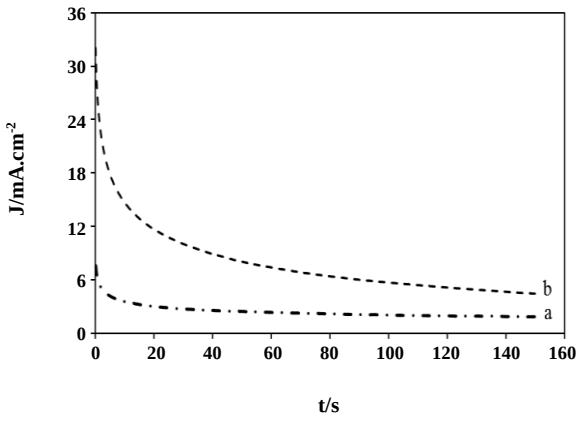

Fig. 5: Chronoamperograms on the (a) GC/PdNPs-CH and (b) GC/PdNPs-$SrFeO_{3-\delta}$NPs-CH electrode at 0.8 V for 0.23 M ethanol oxidation in 1 M KOH.

Controlled potential coulometry (chronoamperometry)

The effect of $SrFeO_{3-\delta}$NPs addition to nanocomposite for electrode modification on the anodic peak current density of ethanol oxidation was studied by chronoamperometry technique. Typical, chronoamperograms for the modified electrodes by PdNPs-CH composite with and without $SrFeO_{3-\delta}$NPs were recorded at a potential value of 0.8 V in 0.23 M ethanol and 1 M KOH solution, is exhibited in Fig. 5. As it was evident in the absence and presence of $SrFeO_{3-\delta}$NPs, the current-time curve was crossed at 7.55 and 32.03 mA/cm^2 amounts of current density at start time, respectively.

The similar CPC curves were obtained for methanol and isopropanol on two types of modified electrodes. Also, the more initial decay of current density could be observed for modified electrode without $SrFeO_{3-\delta}$NPs than GC/PdNPs-$SrFeO_{3-\delta}$NPs-CH electrode. The amount of exchanged charge is associated with the area under the curve. The chronoamperograms show that the exchanged charge was increased in the presence of $SrFeO_{3-\delta}$NPs. Consequently, the composite containing $SrFeO_{3-\delta}$NPs and PdNPs showed the higher catalytic activity for alcohols ($C_1 - C_3$) oxidation. The results of chronoamperometry technique were consistent with the obtained previous consequences of cyclic voltammetry technique.

Raghuveer et al. [32] suggested that a sequence of the rare earth-like strontium (Sr) show superior tolerance towards poisoning through the reaction intermediates of methanol oxidation reaction compared to that of conventional catalysts of noble metal. Presumably, the lattice oxygen in strontium including an oxide could be considered as active oxygen to remove the intermediates of alcohol oxidation reaction like carbon monoxide. Likewise, *Singh et al.* [29] provided evidence that the presence of Sr^{2+} ions in the perovskite improves the catalytic activity of the oxide towards the alcohol oxidation. They believed that the alcohol (in their work: methanol) dehydrogenation is catalyzed by the Fe (II) / Fe(III) redox couple present in oxide structure during the oxidation process. The above results including the decrease of poisoning rate for the palladium catalyst, improvement of the reaction kinetics with reducing the onset potential and the better exchange current density predicate that the catalytic activity of palladium increases by adding $SrFeO_{3-\delta}$NPs perovskite and introduce the PdNPs-$SrFeO_{3-\delta}$NPs-CH composite as a suitable anodic catalyst for alcohol oxidation.

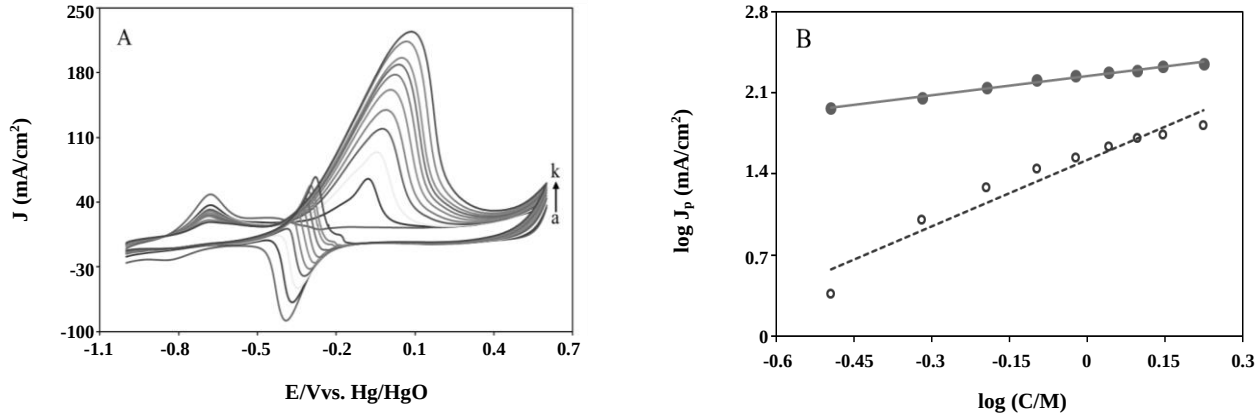

Fig. 6: (A) The cyclic voltammograms at different concentration of methanol: a) 0.00, b) 0.16, c) 0.32, d) 0.48, e) 0.64, f) 0.80, g) 0.95, h) 1.10, i) 1.25, j), 1.40 and k) 1.68 M and (B) Plot of the peak current density dependence vs. the logarithm of methanol concentration at forward (solid) and backward (dash) sweep for methanol oxidation on the GC/PdNPs-$SrFeO_{3-\delta}$NPs-CH electrode in 1M KOH and 50 mV/s scan rate.

Effect of different parameters towards the alcohols oxidation on GC/PdNPs-$SrFeO_{3-\delta}$NPs-CH electrode

We investigated the methanol oxidation on the GC/PdNPs-$SrFeO_{3-\delta}$NPs-CH electrode under the following conditions: alcohol concentration, scan rate and the KOH aqueous solution as an electrolyte.

Alcohol concentration

The effect of increasing the alcohol (C_1-C_3) concentration on the anodic reaction in GC/PdNPs-$SrFeO_{3-\delta}$NPs-CH electrode was investigated in this study. The changes of the anodic current density of methanol oxidation on the GC/PdNPs-$SrFeO_{3-\delta}$NPs-CH electrode in effect of changes of methanol concentration has been shown in Fig. 6A. Apparently, the increasing the methanol concentration up to 1.68 M increases the anodic current density and the current density of methanol oxidation did not have any remarkable increase in methanol concentrations higher than 1.68 M. The oxidation of ethanol and isopropanol had a similar behavior to the methanol oxidation on GC/PdNPs-$SrFeO_{3-\delta}$NPs-CH electrode and. The results show that the anodic current density of ethanol and isopropanol oxidation increases with increasing their concentration up to 0.82 and 0.55 M, respectively. We believe that this effect could be due to the saturation of whole active sites on the nanocomposite surface. Additionally, the reaction of methanol oxidation on the modified electrode is controlled by the diffusion process of methanol towards the catalyst surface. While the methanol concentration increases from 0.16 to 1.68M, the E_f and E_b shift toward the positive direction from -0.08 to +0.09 V and -0.37 to -0.28 V, respectively. The similar results were obtained for ethanol and isopropanol oxidation on the modified electrode. This may be attributed to the poisoning of PdNPs catalyst due to increasing of alcohol concentration and the oxidative removal of the adsorbed intermediates which would shift to a more positive potential. During the cycling process for the different concentration of alcohol (C_1-C_3), the ratio of the forward current density (J_f) to the reverse current density (J_b) caused by methanol oxidation was larger than the ethanol and isopropanol oxidation. It is known that the anodic oxidation peak could be attributed to CO_2 production, and the re-oxidation peak was existed due to intermediate formation [19]. According to Table 1, it is clear that the further accumulation of intermediate species on the surface of the GC/PdNPs-$SrFeO_{3-\delta}$NPs-CH electrode in the ethanol and isopropanol oxidation is expected. Since methanol is the lightest alcohol, its oxidation was relatively with few reaction intermediates. The GC/PdNPs-$SrFeO_{3-\delta}$NPs-CH electrode has minor catalytic effectiveness for ethanol and isopropanol than methanol. The plot of the current density logarithm vs. the alcohol concentration logarithm gives this reaction order [35] with respect to the initial concentration of methanol (Fig. 6B). The reaction order, derived from the slope of the straight line was 0.55 for the positive and 1.91 for the negative sweep for methanol oxidation. The amount of reaction order was calculated for ethanol and isopropanol oxidation reaction that

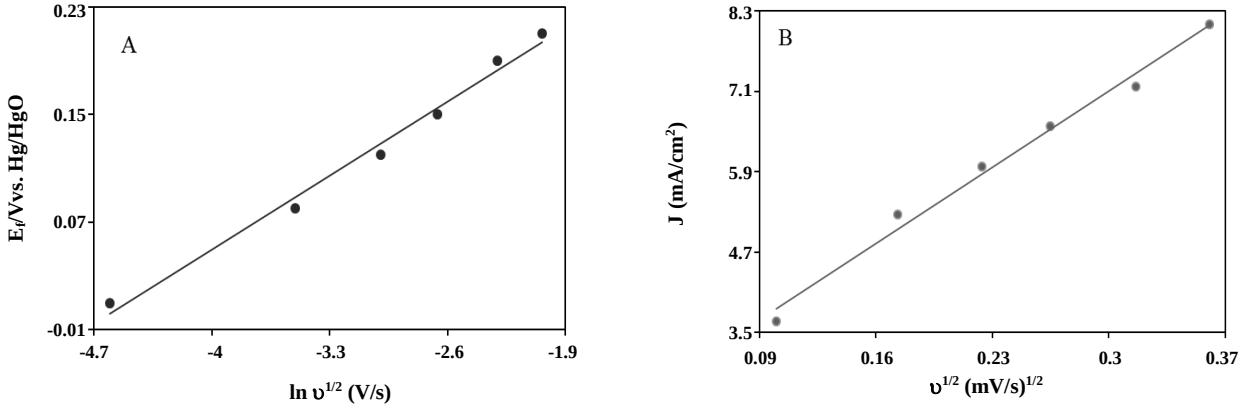

Fig. 7: The plots of (A) the anodic peak potential vs. ln υ and (B) the anodic peak current density of methanol oxidation vs. square root of the scan rate for methanol oxidation on the GC/PdNPs-SrFeO$_{3-\delta}$NPs-CH electrode in 1.68 M methanol and 1 M KOH at different scan rates.

they were 0.92 and 0.98 at the positive, 2.76 and 4.97 at the negative sweep of ethanol and isopropanol oxidation, respectively.

Scan rate

The cyclic voltammograms of 1.68 M methanol oxidation on the GC/PdNPs-SrFeO$_{3-\delta}$NPs-CH electrode in 1 M KOH were recorded at various sweeping rates in the range of 10 - 130 mV/s. Based on these CV curves, the plots of the peak potential vs. ln (υ) (Fig. 7A) and the anodic peak current density amounts of methanol oxidation vs. the square root of the sweeping rate (Fig. 7B) are described. As evident from Fig. 7A, the peak potential of methanol oxidation (E_f) was amplified with increasing the scan rate, and a linear relationship (R^2 = 0.99) has been obtained between E_f and ln (υ). Also, the ethanol and isopropanol oxidation in 1M KOH at various sweeping rates on the GC/PdNPs-SrFeO$_{3-\delta}$NPs-CH electrode show a linear association between E_f and ln (υ). This shows that the alcohol oxidation is an irreversible charge transfer process. The plot of E_p and ln (υ) was a straight line with a slope [36]:

$$\frac{\delta E_p}{\delta(\ln \upsilon)} = \frac{R \times T}{(1-\alpha) \times n \times F} \qquad (11)$$

Where α stands for the coefficient of electron transfer, characterizing the effect of potential on the energy of activation of an electrochemical reaction like alcohol oxidation. The slope of E_p vs. ln (υ) was 0.08 V. The α value was calculated as 0.95 (n = 6 and T = 20 ˚C) which is close to 1.This indicates that the methanol oxidation on GC/PdNPs-SrFeO$_{3-\delta}$NPs-CH electrode has super kinetics. Furthermore, it is clear from Fig.7B that by increasing the functional sweeping rate, the current density of anodic peak of methanol oxidation has been enlarged. This behavior was obvious for ethanol and isopropanol oxidation at various sweeping rates. The linear relationship (R^2 = 0.99) between the square root of the scan rate (υ) and the peak current density indicates that the overall alcohol oxidation reaction is controlled via mass transport of the alcohol from the bulk solution to the electrode surface [37].

Electrolyte concentration

The oxidation of methanol was done on GC/PdNPs-SrFeO$_{3-\delta}$NPs-CH electrode in different concentrations of KOH solution in the range of 0.25 to 1.5 M and the corresponding results are shown in Fig. 8. The best result including the upper current density and the less potential of the anodic peak for the same amount of PdNPs and SrFeO$_{3-\delta}$NPs was shown with 1.5 M KOH. It is due to the CH solubility that depends on the pH of the media. CH polymer can be soluble in acidic solutions (< pH 6). This is because CH can be considered a strong base as it possesses primary amino groups with pK_a = 6.30. The presence of the amino groups indicates that pH substantially alters the charged state and properties of CH. At low pH, these amino groups get protonated and become charged, positively. This makes CH polymer a water-soluble cationic polyelectrolyte. As the pH increases above 6, polymer's amines become

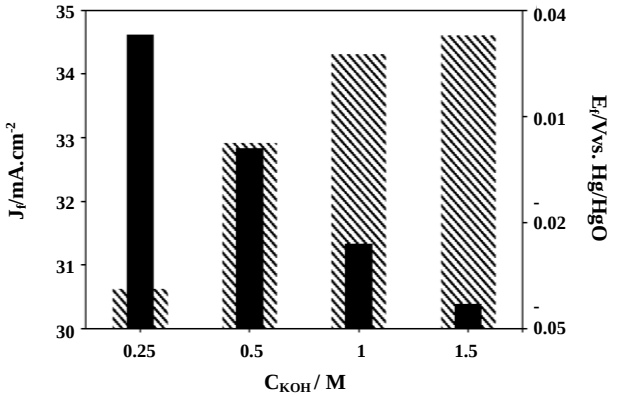

Fig. 8: Effect of KOH concentration on the anodic current density (dash box) and potential (solid box) for 0.32 M methanol oxidation on the GC/PdNPs-SrFeO$_{3-\delta}$NPs-CH electrode.

deprotonated and the CH loses its charge and becomes insoluble [19]. Also, the ionic conductivity of Nafion membranes increases with the increasing of KOH concentration. Consequently, the highest power density is expected to be observed at the higher KOH concentrations. Similar results have also been reported by *Hou et al* [36].

Fuel cell performances

In order to investigate the improved performance of the PdNPs-SrFeO$_{3-\delta}$NPs-CH catalyst as an oxygen storage component, the investigations of the fuel cell were carried out for the MEA made as the anode, and the PtNPs-CH catalyst as the cathode for CH_3OH/O_2. The performance of the proposed fuel cell system (in form of a single cell) depends on the effectiveness of total reaction at the interface between the solid phase of electrodes surface (cathode and anode) and therefore, gas and liquid phases in cathode and anode sides, the temperature of the fuel cell, a methanol concentration of carrier stream and concentration of NaOH in the carrier stream has major effects and has to be optimized.

In order to investigate the temperature effect on the performance of the single cell, various temperatures ranging from 60 - 90 ˚C (P_{O2}= 2 bar; C_{Methanol} = 1 M; flow rate = 1.6 ml/min; C_{NaOH} = 0 M and Nafion® 117 membrane) were tested. The results have been shown in Fig. 9A. From the *I–V* characteristics, the maximum power density of the single cells was obtained 17.71 mW/cm^2 at 70 °C. The Open Circuit Voltage (OCV) of single cells was obtained between 1.28 to 1.56 V for fuel cell temperature ranging from 60 - 90 ˚C.

The flow rates of methanol solution as fuel have a significant effect on the *I–V* characteristics of the single cell. The results of the system were evaluated for different flow rates: 1.6, 2.3 and 3.8 mL/min (P_{O2}= 2 bar; C_{Methanol} = 1 M; C_{NaOH} = 0 M; T = 70 ˚C and Nafion® 117 membrane).The results are shown in Fig. 9B. At given experimental conditions, the power density was decreased as the fuel flow rate was increased from 1.6 to 3.8 ml/min. On the other hand, the OCV was changed slightly by increasing flow rate.

The performance curves of the single cell system were studied for various concentration of methanol solution. Fig. 9C shows the results for PdNPs-SrFeO$_{3-\delta}$NPs-CH catalyst in the DMFC as an anode (P_{O2}= 2 bar; C_{NaOH} = 0 M; flow rate = 1.6 ml/min; T = 70 °C and Nafion® 117 membrane) in 1, 2 and 3 M methanol concentration. As exhibited in Fig. 8C, the power density was decreased with an increase of the methanol concentration from 1 to 3 M. Furthermore, the OCV was changed slightly by increasing the methanol concentration.

The main advantages of the DAFC include faster reaction kinetics of methanol oxidation in an alkaline media than the acidic solution and the potential to use low-priced metal catalysts [39]. It is known that many catalysts reactions (oxygen reduction and methanol oxidation) perform better in alkaline electrolytes. It was also discovered that the methanol oxidation in alkaline electrolytes is structure insensitive [40], It opens up the opportunity for using of perovskite-type oxides [41], which are significantly cheaper than Pd and Pt-based catalysts, in alkaline fuel cells. On the other hand, the current of ionic in the membrane of the alkaline fuel cell can be due to conduction of sodium ions [42].

The experimental results show that in the fuel cell when the pH of fuel is higher, hydrolysis becomes significant and competes with the direct reaction of metal reduction. Metal hydroxides produced from hydrolysis can be reduced to metal (= Sr and Fe) nanoparticles. Due to the formation of intermediate hydroxide phase, the particles formation rate was limited through the reduction reactions of different hydroxides and also their dissolution rates at high *pH*. It is known that CO_2 is a byproduct of DMFC from alcohol oxidation on the anode electrode and can ruin this electrode. One solution can be the carbonation

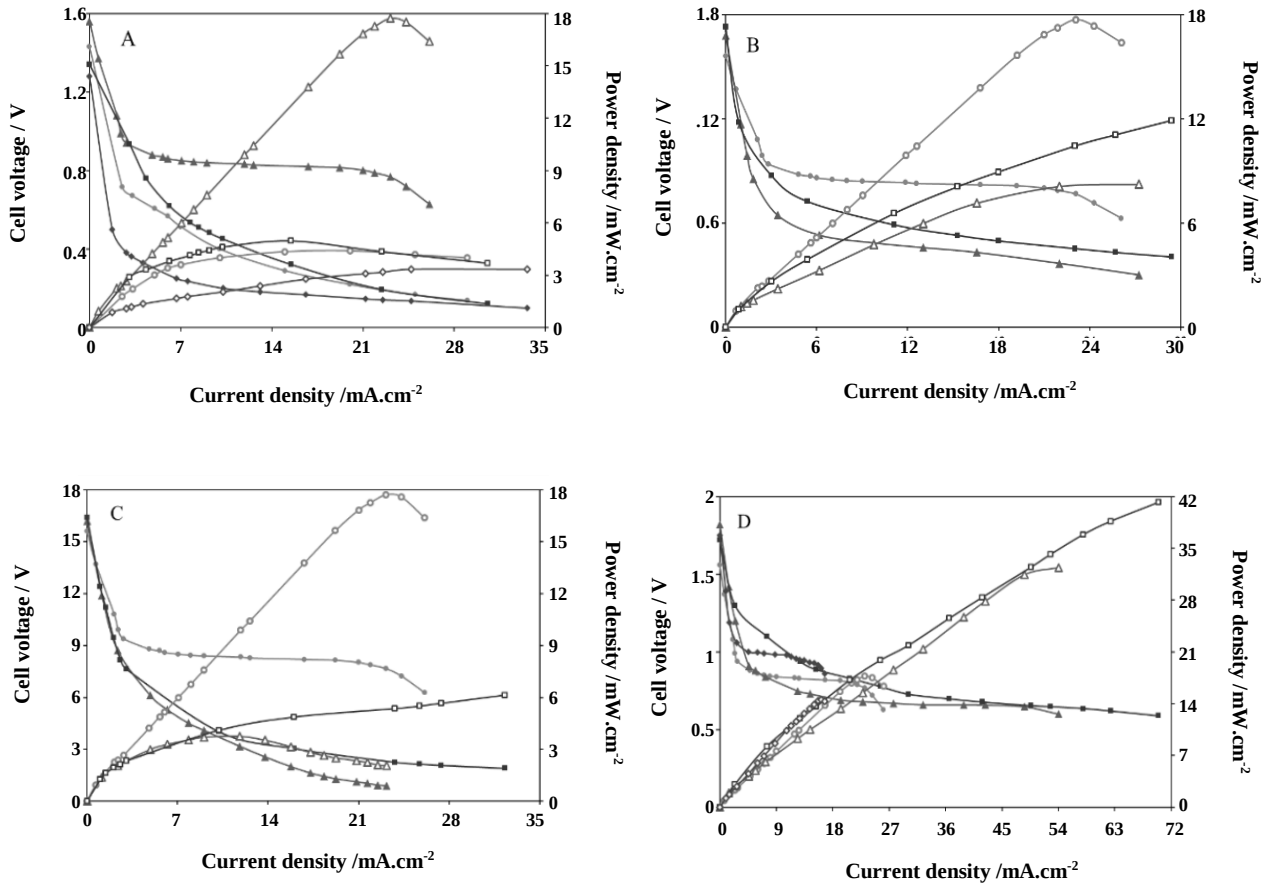

Fig. 9: Electrical performances (Cell voltage (solid) and power density (hollow) against current density) of a 5 cm² DMFC at different (A) temperature (○) 60, (Δ) 70, (□) 80 and (◊) 90 ˚C; (B) methanol flow rate (○) 1.6, (Δ) 2.3 and (□) 3.8 ml/min; (C) methanol concentration (○) 1, (Δ) 2 and (□) 3 M and (D) NaOH concentration (○) 0, (Δ) 1, (□) 1.5 and (◊) 2 M using the PdNPs-SrFeO$_{3-\delta}$NPs-CH/CC-DL anode with P_{O_2} = 2 bar and Nafion® 117 membrane.

of the mentioned electrolyte due to CO_2 production in alkaline electrolytes in alcohol oxidation route as follow:

$$2OH^- + CO_2 \rightarrow CO_3^{2-} + H_2O \quad (12)$$

So, the CO_2 fouling has been decreased with increasing of NaOH concentration. However, carbonate salts to form of the solid precipitation on the anode electrode would increase by increasing of NaOH concentration in the fuel carrier stream, [43]. Consequently, this leads to a reduction in reactivity for alcohol oxidation in the single cell [44]. Therefore, the concentration of NaOH in fuel carrier at alkaline DMFC is very important and must be optimized. Fig. 9D shows the cell performance for PdNPs-SrFeO$_{3-\delta}$NPs-CH catalyst in the DMFC as an anode (P_{O2}= 2 bar; C_{Methanol} = 1 M; flow rate = 1.6 mL/min; T = 70°C and Nafion® 117 membrane) in 0, 1, 1.5 and 2 M NaOH concentration. The open circuit voltage (OCV) of the fuel cell containing PdNPs-SrFeO$_{3-\delta}$NPs-CH electrocatalyst was 1.56 V in 1 M methanol without NaOH, while the corresponding values for alcohol solution containing NaOH with concentration 1, 1.5 and 2 M are about 1.82, 1.72 and 1.75 V, respectively. The DMFC performances of methanol in 1 M NaOH (32.4 mW/cm^2) was better than that of methanol in 0 (17.71 mW/cm^2), 1.5 (41.23 mW/cm^2) and 2 (14.52 mW/cm^2) M NaOH.

Mechanism of methanol oxidation on PdNPs-SrFeO$_{3-\delta}$ NPs-CH nanocomposite

Similar to the mechanism of methanol oxidation on the noble metal surface, it seems that the possible reaction pathway is as follows:

$$Pd + CH_3OH \rightarrow Pd-(CO)_{ads} + 4H^+ + 4e^- \quad (13)$$

$$Pd-(CO)_{ads} + H_2O \rightarrow Pd + CO_2 + 2H^+ + 2e^- \quad (14)$$

It seems that the possible reaction pathway of methanol oxidation on the perovskite $SrFeO_{3-\delta}$ surface in the presence of an alkaline electrolyte be as follows as shown in schematic 2 (M^{n+}: Sr^{2+} and Fe^{3+}) [32].

Based on the suggested mechanism, the catalytic activity of the nanoparticles toward methanol oxidation reaction was affected by both the absorption of methanol molecules as well as the electrical and oxygen ion conductivities of perovskite nanoparticles. The presence of transition metal ions improved the reaction of methanol oxidation. The surface oxygen of the $SrFeO_{3-\delta}$NPs in adjacency of metal particles removed the CO poisoning on the surface of the palladium nanoparticles. Metal hydroxides formed from hydrolysis reaction can be reduced to metal nanoparticles.

SUMMARY AND CONCLUSIONS

In this work, $SrFeO_{3-\delta}$NPs-CH, PdNPs-CH and PdNPs-$SrFeO_{3-\delta}$NPs-CH nanocomposites were successfully synthesized. GC/PdNPs-$SrFeO_{3-\delta}$NPs-CH electrode was prepared as an active electrocatalysts for alcohols (C_1 – C_3) oxidation. Our results showed that the addition of $SrFeO_{3-\delta}$NPs nanoparticles into PdNPs catalyst and the use of a porous matrix of CH polymer can improve the electrode performance for alcohols (C_1 – C_3) oxidation, significantly. The activity of PdNPs-$SrFeO_{3-\delta}$NPs-CH nanocomposite for alcohols (C_1 – C_3) oxidation is higher than that of PdNPs-CH catalyst according to the anodic peak potential and onset potential of methanol oxidation reaction. The factor influencing PdNPs utilization in the methanol oxidation reaction is intrinsically related to PdNPs formation but using $SrFeO_{3-\delta}$NPs helps in enhancing the DMFC performance with low Pd loading.

Acknowledgments

We thank University of Sistan and Baluchestan (USB) for financial support.

Received : May 5, 2016 ; Accepted : Mar. 6, 2017

REFERENCES

[1] Mirabi E., Pishvaie M.R., Abbasian M., Model Reduction of a Solid Oxide Fuel Cell (SOFC) for Control Purposes, *Iran. J. Chem. Chem. Eng. (IJCCE),* **32** (3): 91-105 (2013).

[2] Umeda M., Sugii H., Uchida I., Alcohol Electrooxidation at Pt and Pt–Ru Sputtered Electrodes under Elevated Temperature and Pressurized Conditions, *J. Power Sources* **179** (2):489–496 (2008).

[3] Santasalo A., Vidal-Iglesias F.J., Solla-Gullón J., Berná A., Kallio T., Feliu J.M., Electrooxidation of Methanol and 2-Propanol Mixtures at Platinum Single Crystal Electrodes, *Electrochim. Acta* **54** (26):6576–6583 (2009).

[4] Seweryn J., Lewera A., Electrooxidation of Ethanol on Carbon-Supported Pt–Pd Nanoparticles, *J. Power Sources* **205** (1):264–271 (2012).

[5] Wang Q., Lu X., Xin Q., Sun G., Polyol-Synthesized Pt2.6Sn1Ru0.4/C as a High-Performance Anode Catalyst for Direct Ethanol Fuel Cells, *Chin. J. Catal.* **35** (8):1394–1401 (2014).

[6] Serov A.A., Cho S.Y., Han S., Min M., Chai G., Nam K.H., Kwak C., Modification of Palladium-Based Catalysts by Chalcogenes for Direct Methanol Fuel Cells, *Electrochem. Commun.* **9** (8):2041–2044 (2007).

[7] Su Y.Z., Zhang M.Z., Liu X.B., Li Z.Y., Zhu X.C., Xu C.W., Jiang S.P., Development of Au Promoted Pd/C Electrocatalysts for Methanol, Ethanol and Isopropanol Oxidation in Alkaline Medium, *Int. J. Electrochem. Sci.*, **7**(5): 4158–4170 (2012).

[8] Grace A.N., Pandian K., Pt, Pt–Pd and Pt–Pd/Ru Nanoparticles Entrapped Polyaniline Electrodes – A Potent Electrocatalyst Towards the Oxidation of Glycerol, *Electrochem. Commun.*, **8** (8):1340–1348 (2006).

[9] Abbasi R., Farhadi Kh., Banisaeid S., Nowroozi Pesyan N., Jamali A., Rahmani F., Electrosynthesized Polytyramine-Copper Oxalate Nanocomposite on Copper Electrode for Electrocatalytic Oxidation of Methanol in Alkaline Medium, *Chin. J. Catal.* **35** (7):1098–1104 (2014).

[10] Lee J.M., Han S.B., Lee Y.W., Song Y.J., Kim J.Y., Park K.W., RuO_2–SnO_2 Nanocomposite Electrodes for Methanol Electrooxidation, *J. Alloy Compd.*, **506**(1):57–62 (2010).

[11] Li C.L., Wang C.L., Lin Y.C., Pd-Integrated Lanthanum-Transition Metal Perovskites for Methanol Partial Oxidation, *Catal. Today* **174** (1):135–140 (2011).

[12] Varma A., Deshpande K., Mukasyan A., High Throughput Evaluation of Perovskite-BasedAnode Catalysts for Direct Methanol Fuel Cells, *J. Power Sources*, **158** (1):60-68 (2006).

[13] Mukasyan A.S., Lan A., Complex $SrRuO_3$–Pt and $LaRuO_3$–Pt Catalysts for Direct Alcohol Fuel Cells. *Ind. Eng. Chem. Res.* **47** (1):8989-8994 (2008).

[14] Noroozifar M., Yavari Z., Khorasani-Motlagh M., Ghasemi T., Rohani-Yazdi S.H., Mohammadi M., Fabrication and Performance Evaluation of a Novel Membrane Electrode Assembly for DMFCs, *RSC Adv.*, **6** (1):563-574 (2016).

[15] Yavari Z., Noroozifar M., Khorasani-Motlagh M., Multifunctional Catalysts Toward Methanol Oxidation in Direct Methanol Fuel Cell, *J. Appl. Electrochem.* **45** (5):439-451 (2015).

[16] Noroozifar M., Khorasani-Motlagh M., Yavari Z., Effect of Nano-TiO_2 Particles on the Corrosion Behavior of Chromium-Based Coatings, *Int. J. Nanosci. Nanotechnol.*, **9** (2):85-94 (2013).

[17] Xu Ch., Cheng L., Shen P., Liu Y., Methanol and Ethanol Electrooxidation on Pt and Pd Supported on Carbon Microspheres in Alkaline Media, *Electrochem. Commun.*, **9** (5):997–1001 (2007).

[18] Honda K., Yoshimura M., Rao T.N., Tryk D.A., Fujishima A., Yasuib K., Sakamoto Y., Nishio K., Masuda H., Electrochemical Properties of Pt-Modified Nano-Honeycomb Diamond Electrodes, *J. Electroanal. Chem.*, **514** (1-2):35–50 (2001).

[19] Noroozifar M., Khorasani-Motlagh M., Ekrami-Kakhki M.S., Khaleghian-Moghadam R., Electrochemical Investigation of Pd Nanoparticles and MWCNTs Supported Pd Nanoparticles-Coated Electrodes for Alcohols (C_1–C_3) Oxidation in Fuel Cells, *J. Appl. Electrochem.*, **44** (2):233–243 (2014).

[20] Habibi B., Aluminum Supported Palladium Nanoparticles: Preparation, Characterization and Application for Formic Acid Electrooxidation, *Int. J. Hydrogen Energy*, **38** (13):5464–5472 (2013).

[21] Venkateswara RaO Ch., Singh S.K., Viswanathan B., Electrochemical performance of nano-SiC prepared in thermal plasma. *Indian. J. Chem. A* **47**: (11)1619-1625 (2008).

[22] Wang H., Xu C., Cheng F., Jiang S., Pd Nanowire Arrays as Electrocatalysts for Ethanol Electrooxidation, *Electrochem. Commun.*, **9** (1): 1212–1216 (2007).

[23] Yavari Z., Noroozifar M., Khorasani-Motlagh M., The Improvement of Methanol Oxidation Usingnano-Electrocatalysts. *J. Exp. Nanosci.* **11**(10):798-815 (2016).

[24] Chen Y., Bai L., Zhou C., Lee J.M., Yang Y., Palladium-Catalyzed Aerobic Oxidation of 1-Phenylethanol with an Ionic Liquid Additive, *Chem. Commun.* **47** (22): 6452-6454 (2011).

[25] Alvarez G.F., Mamlouk M., Senthil Kumar S.M., Scott K., Preparation and Characterisation of Carbon-Supported Palladium Nanoparticles for Oxygen Reduction in Low Temperature PEM Fuel Cells, *J. Appl. Electrochem.*, **41** (8):925-937 (2011).

[26] Barakat N.A.M., Motlak M., Kim B.S., El-Deen A.G., Carbon Nanofibers Doped by Ni_xCo_{1-x} Alloy Nanoparticles as Effective and Stable Non Precious Electrocatalyst for Methanol Oxidation in Alkaline Media, *J. Mol. Catal. A Chem.*, **394**:177–187 (2014).

[27] Zhou C., Wang H., Liang J., Peng F., Yu H., Yang J., Effects of RuO_2 Content in Pt/RuO_2/CNTs Nanocatalyst on the Electrocatalytic Oxidation Performance of Methanol, *Chin. J. Catal.*, **29**(11): 1093–1098 (2008).

[28] Ganesan R., Lee J.S., An Electrocatalyst for Methanol Oxidation Based on Tungsten Trioxide Microspheres and Platinum, *J. Power Sources*, **157**(1): 217–221 (2006).

[29] Singh R.N., Sharma T., Singh A., Anindita, Mishra D., Tiwari S.K., Perovskite-type $La_{2-x}Sr_xNiO_4$ ($0 \le x \le 1$) as Active Anode Materials for Methanol Oxidation in Alkaline Solutions, *Electrochim. Acta*, **53** (5): 2322–2330 (2008).

[30] Léger J.M., Preparation and Activity of Mono- or Mi-metallic Nanoparticles for Electrocatalytic Reactions, *Electrochim. Acta*, **5**0(15): 3123–3129 (2005).

[31] Miao F., Tao B., Sun L., Liu T., You J., Wang L., Chu P.K., Preparation and Characterization of Novel Nickel–Palladium Electrodes Supported by Silicon Microchannel Plates for Direct Methanol Fuel Cells, *J. Power Sources* **195** (1):146–150 (2010).

[32] Raghuveer V., Thampi K.R., Xanthopoulos N., Mathieu H.J., Viswanathan B., Rare Earth Cuprates as Electrocatalysts for Methanol Oxidation, *Solid State Ionics*, **140**:263–274 (2001).

[33] Tripković A.V., Popović K.D., Lović J.D., Jovanović V.M., Kowal A., Methanol Oxidation at Platinum Electrodes in Alkaline Solution: Comparison between Supported Catalysts and Model Systems, *J. Electroanal. Chem.*, **572** (1): 119-128 (2004).

[34] Jiang J., Aulich T., High Activity and Durability of Pt Catalyst Toward Methanol Electrooxidation in Intermediate Temperature Alkaline Media, *J. Power Sources* **209**:189–194 (2012).

[35] Becerık İ., Sūzer Ş., Kadirgan F., Electrooxidation of Methanol on Doped Polypyrrole Films in Acidic Media, *J. Electroanal. Chem.*, **502**:118–125 (2001).

[36] Tong H., Li H.L., Zhang X.G., Ultrasonic Synthesis of Highly Dispersed Pt Nanoparticles Supported on MWCNTs and Their Electrocatalytic Activity Towards Methanol Oxidation, *Carbon*, **45**(12): 2424–2432 (2007).

[37] Azizi S.N., Ghasemi Sh., Salek Gilani N., An Electrode with Ni (II) Loaded Analcime Zeolite Catalyst for the Electrooxidation of Methanol, *Chin. J. Catal.*, **35**:383–390 (2014).

[38] Hou H., Wang S., Jin W., Jiang Q., Sun L., Jiang L., Sun G., KOH Modified Nafion112 Membrane for High Performance Alkaline Direct Ethanol Fuel Cell, *Int. J. Hydrogen Energy*, **36** (3):5104-5109 (2011).

[39] Kim J., Momma T., Osaka T., Cell Performance of Pd–Sn Catalyst in Passive Direct Methanol Alkaline Fuel Cell Using Anion Exchange Membrane, *J. Power Sources*, **189** (2):999–1002 (2009).

[40] Chen Y., Zhuang L., Lu J., Non-Pt Anode Catalysts for Alkaline Direct Alcohol Fuel Cells, *Chin. J. Catal*, **28** (10):870-874 (2007).

[41] Miyazaki K., Sugimura N., Matsuoka K., Iriyama Y., Abe T., Matsuoka M., Ogumi Z., Perovskite-Type Oxides $La_{1-x}Sr_xMnO_3$ for Cathode Catalysts in Direct Ethylene Glycol Alkaline Fuel Cells, *J. Power Sources*, **178** (2):683-686 (2008).

[42] Yu E.H., Krewer U., Scott K., Principles and Materials Aspects of Direct Alkaline Alcohol Fuel Cells, *Energies*, **3** (8):1499-1528 (2010).

[43] Gūlzow E., Alkaline Fuel Cells: A Critical View, *J. Power Sources*, **61** (1-2):99-104 (1996)

[44] Wang Y., Li L., Hu L., Zhuang L., Lu J., Xu B., A Feasibility Analysis for Alkaline Membrane Direct Methanol Fuel Cell: Thermo-Dynamic Disadvantages Versus Kinetic Advantages, *Electrochem. Commun.*, **5** (8):662–666 (2003).